HHS Public Access

Author manuscript

Colloids Surf B Biointerfaces. Author manuscript; available in PMC 2017 October 03.

Published in final edited form as:

Colloids Surf B Biointerfaces. 2011 November 01; 88(1): 31–38. doi:10.1016/j.colsurfb.2011.05.044.

Permeability of anti-fouling PEGylated surfaces probed by fluorescence correlation spectroscopy

Charlisa R. Daniels[a], **Carmen Reznik**[a], **Rachel Kilmer**[a], **Mary Jane Felipe**[b], **Maria Celeste R. Tria**[b], **Katerina Kourentzi**[c], **Wen-Hsiang Chen**[c], **Rigoberto C. Advincula**[b,c], **Richard C. Willson**[c], and **Christy F. Landes**[a,*]

[a]Department of Chemistry, Rice University, Houston, TX 77251, United States

[b]Department of Chemistry, University of Houston, Houston, TX 77004, United States

[c]Department of Chemical and Biomolecular Engineering, University of Houston, Houston, TX 77004, United States

Abstract

The present work reports on *in situ* observations of the interaction of organic dye probe molecules and dye-labeled protein with different poly(ethylene glycol) (PEG) architectures (linear, dendron, and bottle brush). Fluorescence correlation spectroscopy (FCS) and single molecule event analysis were used to examine the nature and extent of probe–PEG interactions. The data support a sieve-like model in which size-exclusion principles determine the extent of probe–PEG interactions. Small probes are trapped by more dense PEG architectures and large probes interact more with less dense PEG surfaces. These results, and the tunable pore structure of the PEG dendrons employed in this work, suggest the viability of electrochemically-active materials for tunable surfaces.

Keywords

Fluorescence correlation spectroscopy (FCS); Surface interactions; Poly(ethylene glycol) (PEG); Surface modification; Dynamics

1. Introduction

The present work reports on *in situ* observations of the interaction of various probe molecules with PEGylated surfaces. Poly(ethylene glycol) (PEG) is used in a variety of surface preparations because of its hydrophilicity, low toxicity, and its suppression of nonspecific protein adsorption [1–7]. Despite the wide use of PEGs in dental, ophthalmological, and surgical applications for anti-fouling purposes, a greater molecular-scale understanding of its mechanism of activity is still desirable. Given the structural and applications evidence for the relationship between structure and function in PEGylated surfaces [5,8–10], it is important to pursue an understanding of how various PEGylated surfaces resist nonspecific protein adsorption [11]. More broadly, a better molecular-scale

*Corresponding author. Tel.: +1 713 348 4232; fax: +1 713 348 5155. cflandes@rice.edu (C.F. Landes).

description of transport at soft interfaces would benefit both ion-exchange and size exclusion chromatographic separations sciences [12,13], and the scientific understanding of chromatography, therapeutic separations, biosensors, and immunoassays.

X-ray photoelectron spectroscopy, ellipsometry, fluorescence spectroscopy, theoretical modeling and other techniques extensively support the anti-fouling properties of PEGylated surfaces [6–9,11,14–23]. However, questions remain about the dynamics and mechanisms that direct how these surfaces serve as a physical barrier, decrease adsorption events, and/or repel proteins. It is likely that the mechanism underlying function of soft PEG interfaces is more complicated than a simple physical barrier. The mechanism may depend on the polymer chemistry involved in the fabrication of the surface, including methods involving end-grafting to a surface, radical-initiated polymerization, cross-linking and co-block polymerization [24–26]. These methods of chemical synthesis can produce products that vary in length, density, and architecture.

Both polymer length and shape appear to be important parameters for controlling surface properties. All chain lengths show some resistance to nonspecific protein adsorption [5,10,11,27–31]. Short oligo(ethylene glycols) (OEGs), of fewer than 11 monomers [32], decrease the van der Waals interactions between the surface and protein [30] and offer a layer of water protection [33]. Longer PEGs have been reported to operate based on steric repulsion, chain flexibility, hydrophobic forces, and entropic costs [6,7,14,34]. Polymer shape also contributes to functionality, as cross-linked star-shaped polymers have been observed to be superior in the reduction of nonspecific protein adsorption due to the dense matrix of chains on the surface [35,36]. Bottle-brush polymers have an intricate layering of “bristles” that presents a thicket of PEG chains [22,37]. Apart from the chemical and steric repulsive forces listed above, sieve-like behaviors have been observed in cyclic voltammetry studies [10], in which molecules have been observed to permeate both low and high molecular weight (MW) polymers.

In the present work, a variety of PEG brushes are studied, including linear, dendron, and bottle brush PEGs. For simplicity, the term PEG will be used for both higher MW PEGs and lower MW OEGs, and length differences will be explained in the text. We used confocal FCS and single event analysis to quantify the presence and extent of interactions between PEG and the cationic Rhodamine 6G (R6G) and anionic AlexaFluor 555® (Alexa) dyes as a function of distance from the surface. We have successfully used these techniques to study transport at charged and crowded interfaces and with heterogeneous mixtures [38–41]. Others have recently reported the successful use of FCS to understand probe–polymer brush interactions [42]. When measuring close to the substrate interface, it is important to consider dye–surface interactions [38]. In order to offer insight into these questions we report evidence of the interaction of small molecules and proteins with linear and other forms of PEG brushes (Fig. 1).

We have also used novel electroactive PEG dendrons [43] to modify the pore size (distance between PEG chains) near the surface in efforts to study the tuning of the molecular sieve. FCS analysis of translational diffusion of the dyes in the presence of the polymer revealed two distinct components: a fast, bulk-like component and a slow, hindered component. By

comparing diffusion times for the R6G and Alexa dyes under the various conditions, it was found that interactions with the polymer contribute significantly to diffusion rates measured by FCS out to a focal position of at least 1.0 μm from the glass surface. Similar studies on PEG dendrons support a physical sieve-like model for molecular diffusion near PEGylated interfaces. Lastly, we explored biocompatibility with the protein α-lactalbumin.

2. Results and discussion

2.1. Single versus multiple species analysis

Single-component diffusion algorithms are sufficient for describing dye diffusion near a glass interface. This is illustrated in Fig. 2(a and b) for R6G and Alexa, respectively. As it has been described previously [38], the cationic R6G dye exhibited coulombic interactions with the glass while the anionic Alexa dye did not measurably interact with the surface. This can be seen in comparisons of the measurement close to and including the surface (0.5 μm, see in Section 4 describing geometry of focal volume) versus within the bulk solution (2.0 μm). However, analysis of experiments for the present interfacial measurements required a more sophisticated fitting algorithm, as discussed below.

2.2. Diffusion in the presence of PEG

FCS was used to examine translational diffusion of free dyes in the presence of the linear PEG-functionalized surface depicted in Fig. 1(a). In these studies, the observed autocorrelation curves clearly indicate the presence of both free diffusion and hindered diffusion components. The two distinct diffusion regimes are obvious in the data analysis, as shown in Fig. 3. Two-component analysis [44,45] quantifies the fast component, which indicates free diffusion in bulk solution, and a slower component that indicates interaction between the dye and the PEG ylated surface. The fast component was comparable to the measured diffusion constant for R6G in water. The characteristic bulk diffusion times were 21 ± 2 μs and 21 ± 3 μs for the hard (glass) and soft (PEGylated) surface measurements, respectively.

Hindered diffusion due to interaction with polymer brush–solvent interfaces has recently been attributed to coupling to surface polymer modes [42]. Other possible explanations include coulombic forces between the dye and the PEG, and chemical interactions such as hydrogen bonding or hydronium/hydroxide ion adsorption [46]. Distinguishing between each of these interactions was tested by following the relative contribution of surface diffusion in the confocal observation volume as a function of depth and altered solution chemistry. Thus, additional analyses were performed at various distances from the cover slip surface, as well as in different solution conditions, as discussed below.

Depth-dependent measurements were performed using both cationic R6G and anionic Alexa dyes in neutral, aqueous solvent. As expected, the bulk-like contributions increased as the center of the focal volume was moved further from the surface (Fig. 4). When the observation volume includes the surface (0.5 and 1.0 μm), there is a large contribution of slow diffusion, whereas, further from the surface (1.5 and 2.0 μm), the interaction with the polymer is no longer apparent, as evidenced by the higher contribution of the bulk-like

diffusion component. The changes are observed at distances further than the PEG brush thickness of 40 nm because of the geometry of the focal volume extends to include the polymer layer even when the center of the focus is above the thin-layer (focal height is ~1 μm; see Section 4). The long component is attributed to hindered diffusion. The presence of hindered and bulk diffusion is suggestive of sieve-like behavior of the linear PEG brush. Further experiments were performed to elucidate the nature of this sieve-like behavior.

The diffusion was studied in aqueous (pH 6.0, MB water), electrolytic (0.001 N NaCl), basic (pH 11.0, 0.001 N KOH; pH 8.0, 0.001 N RbOH for Alexa), and acidic (pH 3.0, 0.001 N H_2SO_4) conditions (Fig. 4). The most striking observation is that acidic conditions most strongly decrease hindered diffusion of the cationic dye (Fig. 4(a)), whereas basic conditions most strongly decrease hindered diffusion of the anionic dye (Fig. 4(b)). There are several possible explanations for the observed changes in diffusion characteristics. First, it is possible that changes to the PEG structure or chemistry are the primary force driving the observed surface interactions. Next, it is possible that changes to the dye structure or effective dye size are primarily responsible. Finally, Coloumb interactions could play a role. The elimination of surface interactions in acidic solution for R6G and basic solution for Alexa is strong evidence that the primary driving force does not change in PEG structure, as any ionic effects on the neutral PEG brush would be reflected in similar fashion regardless of the identity of the dye probe at the concentration of the measurements [47–49]. However, the intermediate effects of KOH on the cationic dye diffusion (Fig. 4(a)) suggest that PEG chemistry/structure does play some role. Another potential factor, the alternation of the dye chemistry due to photochemistry or diffusion behavior, can be ruled out because the dye absorption/emission spectra remain independent of pH over a large range [50,51]. An additional possible mechanism is the displacement of the native counterion of the dye. A larger counterion could explain the change in occurrence of hindered diffusion and is consistent with a sieve-like model for the PEG brush structure–function relationship.

The dyes, in the solution conditions that reduce PEG interactions, are solvated by different ions than in their native salt form. R6G is received as a chloride salt. The hydration shell of chloride is reported to be smaller than that of sulfate, with the radii reported as 5.79 and 5.76 Å, respectively [52]. However, since sulfate is a divalent ion, it will coordinate with two dye molecules, resulting in a hydrodynamic radius that is more than twice the size of the original salt. Thus, a larger coordination shell and resulting size exclusion are a likely explanation for the elimination of hindered diffusion in R6G under acidic conditions.

Alexa is received as a sodium salt; the potassium cation of the KOH is larger, as well. Computational studies have reported that the hydrated shell radii of sodium and potassium are 2.37 and 2.80 Å, respectively [53]. However, the relative size change of the newly complexed dyes cannot explain the observed results for Alexa because the inclusion of the rubidium ion, with an even larger ionic radius, does not eliminate hindered diffusion (Fig. 4(b)). The strong size exclusion is limited to the KOH conditions. Additionally, some decrease in hindered diffusion in KOH conditions is observed with the cationic R6G dye (Fig. 4(a)).

A more likely explanation for the slower diffusion rates in the presence of potassium ion is its complexation by PEG chains, which can act as pseudo-crown ethers, with an especially tuned affinity for potassium ions [54,55]. This complexation can cause the PEG chains to shrink, thus excluding the dye from the PEG brush, and can be observed in the hydroxide measurements of both dyes (Fig. 4), but more dramatically with the Alexa dye. As mentioned above, experiments with another alkaline hydroxide, RbOH, confirm that the potassium hydroxide data are anomalous. Thus, the results on linear PEG brushes, in addition to earlier studies [10,56,57], confirm that PEG brushes are not physical barriers. Instead, the results support a model wherein linear PEG brushes are permeable, comprise sieve-like structures with which solutes can interact, and that the extent of interaction can be controlled by either changing the solute size or changing the sieve size. The size exclusion hypothesis can be further tested using PEG dendrons, which allow controllable cavity spacing by the degree of branching of the polymer. An explanation of these findings follows.

2.3. Diffusion in the presence of varying pore sizes

In these experiments, the PEGylated dendrons depicted in Fig. 1(b–e) were used to test the hypothesis of size-dependent, sieve-like behavior for PEG brushes. Because R6G exhibits surface dependent diffusion and photophysics [38,58,59], Alexa was chosen as the primary probe for these studies. Four generations of Janus-type linear-dendrons were analysed. The ellipsometric thicknesses of each brush were 0.9, 1.4, 2.8, and 1.8 ± 0.1 nm for G0–G2, and G1B, respectively. As the dendron generation proceeds from G0 to G2, the density of PEG on the surface decreases due to the spatial requirements of the carbazole on the surface; subsequently, the pore size increases. Theoretical calculations of the pore sizes of the dendritic PEGs have been calculated based on ellipsometric thickness and the MW of the molecules [60]. The grafting densities were 3.4, 2.4, and 1.3 molecules/nm^2 for the G0–G2 surfaces, respectively.

The amount of interaction of the probe with the PEG brush depends strongly on the relative packing densities of the PEG dendrons. The autocorrelation curves for all dendron systems are included in Supplemental Material (Fig. S11). It was found that as the dendron dimension increased from G0 to G2, and the brush density decreased, the probe dye exhibited correspondingly less interaction with the brush surface. This can be seen from the amount of surface diffusion in the autocorrelation curves. The two extreme cases are compared in Fig. 5, wherein the relative amounts of bulk-like diffusion of the G2 and G1B dendrons are shown. The Alexa dye showed no interaction with the G2 dendron, and considerable interactions with the G1B dendron. At all depths, diffusion over the G2 surface matches that of the probe in solution. This observation demonstrates that the least dense G2 dendron brush minimizes probe interactions with the surface. In contrast, the more dense G1B dendron brush exhibited strong probe interactions.

These results demonstrate clearly that, although the PEG chain structure might be preferred for biological applications because of its permeability to water and oxygen, its presence forms sieve-like pores, which can act as traps for diffusing molecules. This property might or might not influence anti-fouling efficacy, as in recent studies, the G2 dendron brush was found to exhibit anti-fouling behavior [43].

2.4. Permeability of bottle brush polymer surfaces

This notion of a sieve-like PEG structure was explored in a more extreme case, in which the bottle-brush PEG, illustrated in Fig. 1(f), was used as the substrate. The bottle brush polymer used in this study has recently been found to display antifouling properties [61]. However, this was measured after incubation, rinsing, and drying of the sample. In our case, we monitored the probe, Alexa, over a surface that had been freshly prepared (‘untreated’) with the dye solution versus a surface that had been allowed to incubate for 2 h in water (‘incubated’). The results can be seen in Table 1. The diffusion time of the ‘incubated’ sample is slower than that of the ‘untreated’ sample. This effect illustrates the strong interactions of the Alexa probe with the bottle-brush.

The extreme hydrophilicity of this system was apparent as the diffusion time of the Alexa probe was found to depend greatly on the exposure time of the sample to water. Our diffusion analyses, the results of which are summarized in Table 1, demonstrate an increase in permeability with exposure time. An increase in permeability as a result of incubation seems to be in contrast with a recent study in which a decrease in protein adsorption was observed for brushes of similar architecture after incubation of the sample [62]. There are two possibilities for the decrease in protein adsorption with surface treatment. One is the possibility that the decrease in adsorption occurred because of the vacuum treatment of the surface in these experiments. Under vacuum conditions, the forced collapse of the polymer may interfere with its preferred architecture. Incubation then allows the polymer to return to its native configuration. In our case, allowing the surface to remain in solution results in added hydration of the brush and possible reorientation of the PEG sidechains. This more flexible, hydrated structure provides more opportunity for the molecules to diffuse through the polymer and interact with the surface. These results show that the methods of measuring protein adsorption do not give a complete picture of the interaction of molecules with a surface. The second possibility is size-exclusion of the proteins from the dense surface, which is discussed below.

2.5. Protein–PEG interactions

The dendrons that resulted in interaction (G2, Fig. 1(d)) and exclusion (G1B, Fig. 1(e)) of the organic dye probe (Fig. 5) were tested with Alexa-labeled α-lactalbumin. The recovered characteristic diffusion times were 636 ± 90 μs and 161 ± 64 μs over the G1B and G2 surfaces, respectively (data not shown). The protein diffuses more slowly than the organic dye, as expected because of its larger size. However, the diffusion times obtained by FCS suggest that the protein exhibits the opposite trend in surface interactions with the two dendron brushes than that observed with the smaller dye probe.

To further assess the permeability of the surfaces, a single molecule blip frequency analysis was performed. Our diffusion data are collected in the time domain, which allows multiple analyses of the trajectories, such as single event (blip) frequency, intensity, and duration values. Fig. 6 displays the average number of events (with standard deviations over three samples) obtained for each acquisition period (trajectories binned up from 10 μs to 100 μs) as a function of distance from the dendronized coverslip surface for the dye-labeled protein (Fig. 6(a)) and the free dye (Fig. 6(b)). In the absence of any interactions between the

dendron-treated surfaces and the probes, the frequency of observed events should be constant regardless of the measurement position, because it reflects the probe concentration, which was constant for the two samples. Blip frequency analysis of the Alexa-labeled α-lactalbumin (Fig. 6(a)) reveals an order of magnitude higher event frequency near the linear G2 brush surface as compared to near the branched G1B brush surface. This indicates that the concentration of protein is higher near the less-dense G2 surface than near the more-dense G1B surface. In direct contrast, similar analysis of the free Alexa dye (Fig. 6(b)) reveals the opposite trend, and thus indicates a higher dye concentration near the G1B surface than near the G2 surface.

Further experiments are underway to assess possible ionic, hydrophobic, and any additional interactions modulating the protein-brush system. In the interim, however, it is possible to make some preliminary assessment of the driving forces. Because both the Alexa-dye and the Alexa-labeled α-lactalbumin are negatively charged under the measurement conditions, it is unlikely that charge–charge interactions are responsible for the opposite trend in interaction with the dendronized surfaces. It seems likely that the difference lies in size-exclusion effects. The G2 dendronized surface offers larger pores with space between the PEG chains, thus allowing the protein to penetrate into and interact with the brush. The smaller free Alexa dye can freely diffuse into and out of the brush. The G1B dendronized surface presents smaller pores, thus excluding the larger protein but trapping the smaller dye. The strong protein–G2 interaction, combined with recent results that demonstrate the increased protein anti-fouling properties of the G2 brush [43], together highlight that anti-fouling properties do not necessarily correlate with exclusion. These experiments further support the sieve-like properties of PEG and illustrate how the degree of permeability is dependent upon both the density of the chains on the surface and the size of the diffusion species. These experiments also illustrate that surface engineering can combine the attributes of these properties to produce an optimum surface for advanced functional surface applications.

3. Conclusions

We have measured the diffusion of cationic and anionic dyes in a variety of PEG structures. Both the cationic and the anionic dyes show a fast and slow component in the autocorrelation analysis. The slow component is evidence of the dye interacting with the polymer. These experiments reveal evidence of PEG pseudo-crown ether behavior in the presence of K, which can be seen in reduced interaction of the dyes with the PEG brush. Additionally, these experiments performed in multiple conditions prove that the PEG brush is permeable. We have also observed what we hypothesize to be size exclusion effects when allowing the dyes to exchange their native counterion for a larger one. In these instances, the dyes with larger hydrodynamic radii are excluded from interaction with the linear PEG. We have varied the pore size of the polymer at the surface with PEG dendrons and observed that density of PEG is also an important parameter. Overall, we found that there is a strong relationship between the probe size, mobility, and density of PEG on the surface. Small probes get trapped by highly dense PEG architectures and exhibit interactions with moderately dense architectures. Large probes readily interact with sparsely populated PEG surfaces and are excluded from dense PEG architectures. The dendrons measured in this

work offer the ability to vary both pore size and PEG density which allows fabrication of tunable surfaces.

4. Experimental

4.1. Materials and linear PEG preparation

Many of the details of the sample preparation, setup, and theory have been previously reported [38–41]. 100 nm orange fluorescent carboxylate-modified FluoSphere beads (max abs/em: 540/560 nm) beads (1:1000 dilution) were used to determine the focal volume for the FCS measurements. Rhodamine 6G (max abs/em: 530/566 nm) and AlexaFluor® 555 (max abs/em: 555/565 nm) were diluted to approximately 100 pM for signal versus concentration optimization. NaCl (5 M, Sigma–Aldrich), KOH (85+%, Sigma-Aldrich), RbOH (Sigma-Aldrich) and spectroscopic grade H_2SO_4 (J.T. Baker) were diluted to a 0.001 N solutions to supply the differing environments for the fluorescent dyes. The basic solutions were pH 11.0 and 8.0; the acidic solution was pH 3.0. Hyclone molecular biology grade (MB) water (VWR) was used for all dilutions. No. 1 coverslips were rinsed in the MB grade water and plasma cleaned in oxygen for 2 min. For PEGylation, the coverslips were pre-treated with an amino-silane linker, Vectabond™ (Vector Laboratories). The reagent was dissolved in acetone and the plasma cleaned slides were submerged followed by a MB water rinse and drying with N_2. An aqueous mixture containing 25% PEG 5000 (Fluka) and 11% $NaHCO_3$ (7.5%, Sigma–Aldrich) was then applied to the cavity of a custom silicon chamber. The mixture was allowed to dry for 4 h, followed by a MB water rinse and drying with N_2. Fig. 1(a) depicts the resulting PEGylated slide. Measurements were taken in each of the four solutions (aqueous, acidic, basic, and electrolytic) and at four depths (0.5, 1.0, 1.5, and 2.0 μm).

4.2. PEG dendron synthesis [43]

The three different generations of PEGylated carbazole linear dendrons, G_0CbztEG, G_1CbztEG and G_2CbztEG, were synthesized (Schemes S1 and S2) by first preparing the three different generations of carbazole-terminated dendrons made through a sonochemical Mitsonobu type etherification method [63,64]. The carbazole carboxylic acid dendrons were then functionalized with tetraethylene glycol units via dicyclohexylcarbodiimide coupling. ^{1}H NMR and MALDI-TOF spectrometry confirmed the structures of the desired G_nCbztEG molecules (the dendrons are abbreviated as Gn in the remainder of the discussion, with the branched dendron as GnB). Details of the linear-dendron synthesis can be found elsewhere [43]. Fig. 1(b–d) depicts the dendrons, from $n = 0$, 1, and 2. Fig. 1(e) depicts the branched version of $n = 1$.

Thin films were fabricated onto indium tin oxide (ITO) coated cover slips employing an *ex situ* electrochemical polymerization technique, preventing the use of glass coverslips. All electropolymerizations were performed using an Autolab PGSTAT 12 potentiostat (Metrohm) coupled with an SPR instrument (Autolab ESPRIT from Eco Chemie) which was controlled by GPES version 4.9 software provided by MetrOhm and Eco Chemie. The electropolymerization was performed using cyclic voltammetry (CV) in a three-electrode cell containing 20 μM PEGylated carbazole dendron monomers and 0.1 M

tetrabutylammonium hexafluorophosphate (TBAP) as supporting electrolyte in chromatographic grade acetonitrile by sweeping the voltage from 0 V to 1.3 V for 20 cycles at a scan rate of 50 mV/s against a Ag/AgCl non-aqueous reference electrode and Pt counter-electrode.

4.3. PEG bottle brush synthesis [61]

Reagent chemicals were purchased from Aldrich and were used without further purification unless otherwise indicated. Tetrahydrofuran (THF) used in the synthesis and polymerization reactions was distilled from sodium/benzophenone ketyl. Methyl methacrylate (MMA, 99+ %) and poly(ethylene glycol) methyl ether methacrylate (PEGMEMA) (MW 300) monomers, were passed through a column with alternating layers of activated basic alumina and inhibitor remover replacement packing to remove the inhibitor and were stored at −20 °C. The chain transfer agent (CTA), 3,5-bis(4-(9H-carbazol-9-yl)butoxy)benzyl 4-cyano-4-(phenylcarbonothioylthio)pentanoate (Cbz-CTA) was synthesized according to the method reported by Patton et al. [65].

Electrochemical deposition was performed with a Parstat 2263 (Princeton Applied Research) instrument using PowerSuite software. All experiments were carried out using a three-electrode set-up where the ITO cover slip was used as the working electrode, Pt wire as the counter electrode and Ag/AgCl as the reference electrode. Electrodeposition techniques prevented the use of glass coverslips. A solution of the CTA (0.5 mM) and the supporting electrolyte, tetrabutylammonium hexafluorophosphate (TBAH) (0.1 M) in THF was used for preparing the electro-generated CTA film. Potentiostatic experiment was employed to deposit the CTA using a constant potential of 1.4 V for 240 s.

In a typical run, a solution of PEGMEMA (4945 mg, 16.48 mmol), AIBN (0.9 mg, 0.0055 mmol) and 25 mL of dry THF (for PEGMEMA polymerization) were degassed in a Schlenk tube by bubbling with N_2 gas for 30–45 min. The degassed solutions were transferred to another Schlenck tube backfilled with N_2 gas containing the CTA-modified ITO cover slips through a cannula. The flask was placed in a preheated oil bath at 60 °C for 3 h. The slides were then subjected to Soxhlet extraction overnight using THF as solvent to remove any unbound polymers.

4.4. Characterization of the surface

The surfaces were analysed by means of AFM, XPS, CV, and ellipsometry. The analyses of the surfaces are described in Supporting Information.

4.5. Protein labeling and purification

Alexa Fluor® 555 succinimidyl ester (1 mg in dimethylformamide; Invitrogen Corp.) was used to label α-lactalbumin (10 mg; Sigma–Aldrich) in 1 mL of 0.1 M sodium bicarbonate buffer, pH 7.4 to preferentially label the protein amine terminus rather than the ε-amino groups of the lysines, according to the manufacturer's protocol.

The reaction was incubated at room temperature for 1 h under constant mixing, and stopped with 0.1 mL of freshly prepared 1.5 M hydroxylamine, pH 8.5. The labeled protein was

dialyzed against water for 24 h and then against 10 mM Tris, 100 mM NaCl at pH 8 for 24 h.

To ensure complete removal of the unincorporated fluorophore, PD-10 desalting columns and/or gel filtration chromatography was used. Gel filtration was carried out on a Pharmacia FPLC system using Sephadex 10/300 GL (GE Healthcare) with 10 mM Tris and 100 mM NaCl at pH8.0 as running buffer. The fractions with an estimated fluorophore-to-protein ratio of 1 ± 0.2 were used for the studies.

4.6. FCS setup

A solid state laser was the excitation source (VERDI, Coherent). The 532 nm light was circularly polarized, filtered, and expanded to overfill the back aperture of an oil immersion microscope objective (FLUAR 100×, 1.3 NA, Carl Zeiss, GmBH). After excitation, the fluorescence was captured by the same objective [66] and isolated by a dichroic mirror (z532rdc, Chroma Technology) and a notch filter (NHPF-532.0, Kaiser). Fluorescence was then guided through a 50 μm pinhole to block out-of-focus light, increasing spatial resolution [67,68]. The resulting focal volume had a $1/e^2$ beam radius of ~230 nm and height of ~1 μm [68]. Photons were detected by avalanche photodiodes (APD; SPCM-AQR-15, Perkin-Elmer). A piezo stage (P-517.3CL Physik Instrumente) and controller (SPM 100, RHK Technology) allowed the user to maneuver the sample in 3 dimensions. The output from the APDs was split to a photon counting board (PMS-400-A, Boston Electronics Corporation) and a 2D imaging system (RHK Technology). For each condition, the focal volume was calibrated in order to ensure that no experimental condition altered the confocal beam geometry. It was found that the beam geometry was consistent throughout the experiments. The theory of FCS is explained in the Supporting Information document. Additional details of the experiments have been presented previously [38–41].

4.7. Using FCS to measure soft surface interactions [38]

The fluctuating intensity characterized by FCS arises from the motion of fluorescent molecules as they pass through a tightly focused focal volume [69] as shown in Fig. 7, which depicts our sample and observation volume. For this study, measurements were acquired with the focal volume placed first at the surface (Fig. 7, far left), corresponding to an offset of 0.5 μm of the beam waist from the surface, and at successively deeper positions within the sample (Fig. 7, center and far right). Therefore, the findings represent diffusion characteristics of the probes as a function of distance from the functionalized surface. Since the focal volume is ~1 μm in the z dimension, taking measurements in 0.5 μm steps ensures that an overlap of data acquisition is present.

Supplementary Material

Refer to Web version on PubMed Central for supplementary material.

Acknowledgments

The authors would like to thank Roderick Pernites of the Advicula group at University of Houston for his initial characterization work. The Welch Grant E-1264, as awarded to Richard Willson, supported the protein work. C. Landes thanks the Norman Hackerman Welch Young Investigator Program at Rice University. The NSF

CBET-0854979 and Robert A Welch Foundation (E-1551) as awarded to Rigoberto C. Advincula, supported the PEG linear-dendron and bottle brush synthesis and studies. Acknowledgment is also made to the Donors of the American Chemical Society Petroleum Research Fund for partial support of this research.

References

1. Aguilar, GA., Hiza, RJ. Extreme-Pressure Additives for Lubricating Greases Containing Thiadiazoles, Polyoxyalkylenes and Metal Dithiophosphates. US Pat. 20090156444. 2009.
2. Hoffman AS. Non-fouling surface technologies. J Biomater Sci Polym Ed. 1999; 10:1011–1014. [PubMed: 10591129]
3. Brash JL, Horbett TA. Proteins at interfaces. An overview. ACS Symp Ser. 1995; 602:1–23.
4. Ostuni E, Chapman RG, Holmlin RE, Takayama S, Whitesides GM. A survey of structure–property relationships of surfaces that resist the adsorption of protein. Langmuir. 2001; 17:5605–5620.
5. Yang Z, Galloway JA, Yu H. Protein interactions with polyethylene glycol self-assembled monolayers on glass substrates: diffusion and adsorption. Langmuir. 1999; 15:8405–8411.
6. Jeon SI, Andrade JD. Protein–surface interactions in the presence of polyethylene oxide. II. Effect of protein size. J Colloid Interface Sci. 1991; 142:159–166.
7. Jeon SI, Lee JH, Andrade JD, De Gennes PG. Protein–surface interactions in the presence of polyethylene oxide. I. Simplified theory. J Colloid Interface Sci. 1991; 142:149–158.
8. Halperin A, Fragneto G, Schollier A, Sferrazza M. Primary versus ternary adsorption of proteins onto PEG brushes. Langmuir. 2007; 23:10603–10617. [PubMed: 17803323]
9. Schlapak R, Armitage D, Saucedo-Zeni N, Chrzanowski W, Hohage M, Caruana D, Howorka S. Selective protein and DNA adsorption on PLL-PEG films modulated by ionic strength. Soft Matter. 2009; 5:613–621.
10. Schlapak R, Caruana D, Armitage D, Howorka S. Semipermeable poly(ethylene glycol) films: the relationship between permeability and molecular structure of polymer chains. Soft Matter. 2009; 5:4104–4112.
11. Feldman K, Haehner G, Spencer ND, Harder P, Grunze M. Probing resistance to protein adsorption of oligo(ethylene glycol)-terminated self-assembled monolayers by scanning force microscopy. J Am Chem Soc. 1999; 121:10134–10141.
12. Ramsden JJ, Roush DJ, Gill DS, Kurrat R, Willson RC. Protein adsorption kinetics drastically altered by repositioning a single charge. J Am Chem Soc. 1995; 117:8511–8516.
13. Brooks DE, Haynes CA, Hritcu D, Steels BM, Muller W. Size exclusion chromatography does not require pores. Proc Natl Acad Sci USA. 2000; 97:7064–7067. [PubMed: 10852951]
14. Halperin A. Polymer brushes that resist adsorption of model proteins: design parameters. Langmuir. 1999; 15:2525–2533.
15. Knotts TAIV, Rathore N, de Pablo JJ. An entropic perspective of protein stability on surfaces. Biophys J. 2008; 94:4473–4483. [PubMed: 18326646]
16. Hamilton-Brown P, Gengenbach T, Griesser HJ, Meagher L. End terminal, poly(ethylene oxide) graft layers: surface forces and protein adsorption. Langmuir. 2009; 25:9149–9156. [PubMed: 19534458]
17. Prime KL, Whitesides GM. Adsorption of proteins onto surfaces containing end-attached oligo(ethylene oxide): a model system using self-assembled monolayers. J Am Chem Soc. 1993; 115:10714–10721.
18. Sharma S, Johnson RW, Desai TA. XPS and AFM analysis of antifouling PEG interfaces for microfabricated silicon biosensors. Biosens Bioelectron. 2004; 20:227–239. [PubMed: 15308226]
19. Wach JY, Malisova B, Bonazzi S, Tosatti S, Textor M, Zurcher S, Gademann K. Protein-resistant surfaces through mild dopamine surface functionalization. Chem Eur J. 2008; 14:10579–10584. [PubMed: 18924224]
20. Benhabbour, SR., Liu, L., Sheardown, H., Adronov, A. Macromolecules. Vol. 41. Washington, DC, U.S: 2008. Protein Resistance of Surfaces Prepared by Chemisorption of Monothiolated Poly (ethylene glycol) to Gold and Dendronization with Aliphatic Polyester Dendrons: Effect of Hydrophilic Dendrons; p. 2567-2576.

21. Inoue Y, Ishihara K. Reduction of protein adsorption on well-characterized polymer brush layers with varying chemical structures. Colloids Surf B: Biointerfaces. 2010; 81:350–357. [PubMed: 20705439]
22. Olanya G, Thormann E, Varga I, Makuska R, Claesson PM. Protein interactions with bottle-brush polymer layers: effect of side chain and charge density ratio probed by QCM-D and AFM. J Colloid Interface Sci. 2010; 349:265–274. [PubMed: 20579658]
23. Yang H, Shin K, Tae G, Satija SK. Structure of a monolayer of poly(ethylene glycol) end-capped with a fluoroalkyl group and its relationship with protein adsorption at the aqueous interface. Soft Matter. 2009; 5:2731–2737.
24. Advincula RC, Brittain WJ, Baster KC, Ruhe J. Polymer brushes: synthesis, characterization. Applications. 2004
25. Bhat RR, Tomlinson MR, Genzer J. Orthogonal surface-grafted polymer gradients: a versatile combinatorial platform. J Polym Sci Part B: Polym Phys. 2005; 43:3384–3394.
26. Mert O, Doganci E, Erbil HY, Demir AS. Surface characterization of poly(L-lactic) acid-methoxy polyethylene glycol diblock copolymers by static and dynamic contact angle measurements, FTIR and ATR-FTIR. Langmuir. 2008; 24:749–757. [PubMed: 18189428]
27. Harbers GM, Emoto K, Greef C, Metzger SW, Woodward HN, Mascali JJ, Grainger DW, Lochhead MJ. Functionalized polyethylene glycol-based bioassay surface chemistry that facilitates bio-immobilization and inhibits nonspecific protein, bacterial, and mammalian cell adhesion. Chem Mater. 2007; 19:4405–4414. [PubMed: 18815622]
28. Ju H, McCloskey BD, Sagle AC, Kusuma VA, Freeman BD. Preparation and characterization of crosslinked poly(ethylene glycol) diacrylate hydrogels as fouling-resistant membrane coating materials. J Membr Sci. 2009; 330:180–188.
29. Liu SX, Kim JT, Kim S, Singh M. The effect of polymer surface modification via interfacial polymerization on polymer–protein interaction. J Appl Polym Sci. 2009; 112:1704–1715.
30. Zhu B, Eurell T, Gunawan R, Leckband D. Chain-length dependence of the protein and cell resistance of oligo(ethylene glycol)-terminated self-assembled monolayers on gold. J Biomed Mater Res. 2001; 56:406–416. [PubMed: 11372059]
31. Vanderah DJ, Vierling RJ, Walker ML. Oligo(ethylene oxide) self-assembled monolayers with self-limiting packing densities for the inhibition of nonspecific protein adsorption. Langmuir. 2009; 25:5026–5030. [PubMed: 19358588]
32. Vanderah DJ, La H, Naff J, Silin V, Rubinson KA. Control of protein adsorption: molecular level structural and spatial variables. J Am Chem Soc. 2004; 126:13639–13641. [PubMed: 15493920]
33. Li L, Chen S, Zheng J, Ratner BD, Jiang S. Protein adsorption on oligo(ethylene glycol)-terminated alkanethiolate self-assembled monolayers: the molecular basis for nonfouling behavior. J Phys Chem B. 2005; 109:2934–2941. [PubMed: 16851306]
34. Yeh PY, Kainthan RK, Zou Y, Chiao M, Kizhakkedathu JN. Self-assembled monothiol-terminated hyperbranched polyglycerols on a gold surface: a comparative study on the structure, morphology, and protein adsorption characteristics with linear poly(ethylene glycol)s. Langmuir. 2008; 24:4907–4916. [PubMed: 18361531]
35. Heyes CD, Kobitski AY, Amirgoulova EV, Nienhaus GU. Biocompatible surfaces for specific tethering of individual protein molecules. J Phys Chem B. 2004; 108:13387–13394.
36. Heyes Colin D, Groll J, Moller M, Nienhaus GU. Synthesis, patterning and applications of star-shaped poly(ethylene glycol) biofunctionalized surfaces. Mol Biosyst. 2007; 3:419–430. [PubMed: 17533455]
37. Zhou Y, Liedberg B, Gorochovceva N, Makuska R, Dedinaite A, Claesson PM. Chitosan-N-poly(ethylene oxide) brush polymers for reduced nonspecific protein adsorption. J Colloid Interface Sci. 2006; 305:62–71. [PubMed: 17049545]
38. Daniels CR, Reznik C, Landes CF. Dye diffusion at surfaces: charge matters. Langmuir. 2010; 26:4807–4812. [PubMed: 20163084]
39. Reznik C, Darugar Q, Wheat A, Fulghum T, Advincula RC, Landes CF. Single ion diffusive transport within a poly(styrene sulfonate) polymer brush matrix probed by fluorescence correlation spectroscopy. J Phys Chem B. 2008; 112:10890–10897. [PubMed: 18630854]

40. Reznik C, Estillore N, Advincula RC, Landes CF. Single molecule spectroscopy reveals heterogeneous transport mechanisms for molecular ions in a polyelectrolyte polymer brush. J Phys Chem B. 2009; 113:14611–14618. [PubMed: 19813742]
41. Tcherniak A, Reznik C, Link S, Landes CF. Fluorescence correlation spectroscopy: criteria for analysis in complex systems. Anal Chem (Washington, DC, US). 2009; 81:746–754.
42. Wang S, Zhu Y. Molecular diffusion on surface tethered polymer layers: coupling of molecular thermal fluctuation and polymer chain dynamics. Soft Matter. 2010; 6:4661–4665.
43. Felipe MJ, Ponnapati R, Pernites R, Dutta P, Advincula R. Synthesis and electrografting of dendron anchored OEGylated surfaces and their protein adsorption resistance. ACS Appl Mater Interfaces. 2010; 2:3401–3405. [PubMed: 21077629]
44. Haustein E, Schwille P. Ultrasensitive investigations of biological systems by fluorescence correlation spectroscopy. Methods. 2003; 29:153–166. [PubMed: 12606221]
45. Wirth MJ, Ludes MD, Swinton DJ. Analytic solution to the autocorrelation function for lateral diffusion and rare strong adsorption. Appl Spectrosc. 2001; 55:663–669.
46. Kreuzer HJ, Wang RLC, Grunze M. Hydroxide ion adsorption on self-assembled monolayers. J Am Chem Soc. 2003; 125:8384–8389. [PubMed: 12837111]
47. Rubinson KA, Krueger S. Poly(ethylene glycol)s 2000–8000 in water may be planar: a small-angle neutron scattering (SANS) structure study. Polymer. 2009; 50:4852–4858.
48. Capuano F, Vergara A, Paduano L, Annunziata O, Sartorio R. Electrostatic and excluded volume effects on the transport of electrolytes in poly(ethylene glycol) – water “mixed solvents”. J Phys Chem B. 2003; 107:12363–12369.
49. Tan C, Albright JG, Annunziata O. Determination of preferential interaction parameters by multicomponent diffusion. Applications to poly(ethylene glycol)–salt–water ternary mixtures. J Phys Chem B. 2008; 112:4967–4974. [PubMed: 18376888]
50. Misra V, Mishra H, Joshi HC, Pant TC. Excitation energy transfer between acriflavine and rhodamine 6G as a pH sensor. Sens Actuators B: Chem. 2000; 63:18–23.
51. Panchuk-Voloshina N, Haugland RP, Bishop-Stewart J, Bhalgat MK, Millard PJ, Mao F, Leung W, Haugland RP. Alexa dyes, a series of new fluorescent dyes that yield exceptionally bright photostable conjugates. J Histochem Cytochem. 1999; 47:1179–1188. [PubMed: 10449539]
52. Ustinov AN, Afanas’ev VN. Quantitative characteristics of hydration in solutions of sodium sulfate and sodium chloride at 278.15–323.15 K. Zhurnal Neorganicheskoi Khimii. 2008; 53:882–889.
53. Azam SS, Zaheer-ul-Haq, Fatmi MQ. Classical and QM/MM MD simulations of sodium(I) and potassium(I) ions in aqueous solution. J Mol Liq. 2010; 153:95–100.
54. Balasubramanian D, Chandani B. Poly(ethylene glycol): a poor chemist’s crown. J Chem Educ. 1983; 60:77–78.
55. Ono K, Konami H, Murakami K. Conductometric studies of ion binding to poly(oxyethylene) in methanol. J Phys Chem. 1979; 83:2665–2669.
56. Hakem IF, Lal J, Bockstaller MR. Binding of monovalent ions to PEO in solution: relevant parameters and structural transitions. Macromolecules. 2004; 37:8431–8440.
57. Schlapak R, Armitage D, Saucedo-Zeni N, Hohage M, Howorka S. Dense passivating poly(ethylene glycol) films on indium tin oxide substrates. Langmuir. 2007; 23:10244–10253. [PubMed: 17715951]
58. Blom H, Chmyrov A, Hassler K, Davis LM, Widengren J. Triplet-state investigations of fluorescent dyes at dielectric interfaces using total internal reflection fluorescence correlation spectroscopy. J Phys Chem A. 2009; 113:5554–5566. [PubMed: 19374408]
59. Blom H, Hassler K, Chmyrov A, Widengren J. Electrostatic interactions of fluorescent molecules with dielectric interfaces studied by total internal reflection fluorescence correlation spectroscopy. Int J Mol Sci. 2010; 11:386–406. [PubMed: 20386645]
60. Ma H, Wells M, Beebe TP Jr, Chilkoti A. Surface-initiated atom transfer radical polymerization of oligo(ethylene glycol) methyl methacrylate from a mixed self-assembled monolayer on gold. Adv Funct Mater. 2006; 16:640–648.
61. Tria MCR, Grande CDT, Ponnapati RR, Advincula RC. Electrochemical deposition and surface-initiated RAFT polymerization: protein and cell-resistant PPEGMEMA polymer brushes. Biomacromolecules. 2010; 11:3422–3431. [PubMed: 21028799]

62. Zhang Z, Ma H, Hausner DB, Chilkoti A, Beebe TP Jr. Pretreatment of amphiphilic comb polymer surfaces dramatically affects protein adsorption. Biomacromolecules. 2005; 6:3388–3396. [PubMed: 16283770]
63. Kaewtong C, Jiang G, Felipe MJ, Pulpoka B, Advincula R. Self-assembly and electrochemical oxidation of polyamidoamine-carbazole dendron surfmer complexes: nanoring formation. ACS Nano. 2008; 2:1533–1542. [PubMed: 19206356]
64. Taranekar P, Fulghum T, Patton D, Ponnapati R, Clyde G, Advincula R. Investigating carbazole jacketed precursor dendrimers: sonochemical synthesis, characterization, and electrochemical crosslinking properties. J Am Chem Soc. 2007; 129:12537–12548. [PubMed: 17894494]
65. Patton DL, Taranekar P, Fulghum T, Advincula R. Electrochemically active dendritic – linear block copolymers via RAFT polymerization: synthesis, characterization, and electrodeposition properties. Macromolecules. 2008; 41:6703–6713.
66. Koppel DE, Axelrod D, Schlessinger J, Elson EL, Webb WW. Dynamics of fluorescence marker concentration as a probe of mobility. Biophys J. 1976; 16:1315–1329. [PubMed: 974223]
67. Hess ST, Webb WW. Focal volume optics and experimental artifacts in confocal fluorescence correlation spectroscopy. Biophys J. 2002; 83:2300–2317. [PubMed: 12324447]
68. Qian H, Elson EL. Analysis of confocal laser-microscope optics for 3-D fluorescence correlation spectroscopy. Appl Opt. 1991; 30:1185–1195. [PubMed: 20582127]
69. Haustein E, Schwille P. Fluorescence correlation spectroscopy: novel variations of an established technique. Annu Rev Biophy Biomol Struct. 2007; 36:151–169.

Appendix A. Supplementary data

Supplementary data associated with this article can be found, in the online version, at doi: 10.1016/j.colsurfb.2011.05.044.

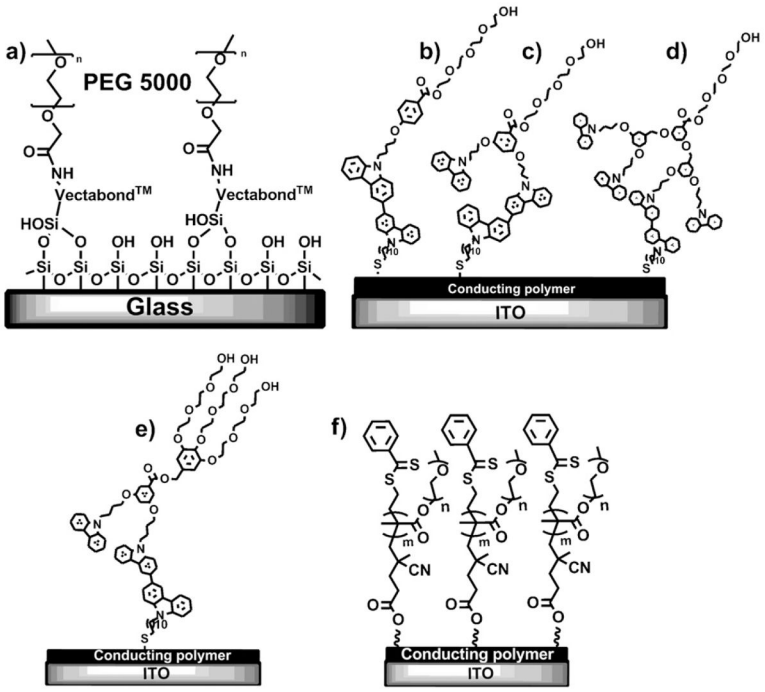

Fig. 1.

Depiction of the surfaces used in this study. All details of surface modification are described in the text. (a) Structure of linear PEG brushes grafted to a glass surface. Additional PEG brushes were prepared with G_n CbztEG Janus-type dendrons on ITO surfaces. Janus-type dendrons are “double-faced” molecules. In this case, one face is the carbozole end, which is grafted onto the ITO surface, and the other face is the PEG chain extended in solution. Dendron generations used in this study include: (b) G_0CbztEG (c), G_1CbztEG (d), G_2CbztEG and (e) branched G_1CbztEG, (the dendrons are abbreviated as Gn in the text, with the branched dendron as GnB), (f) structure of bottle brush polymers, with a PMMA backbone and PEG ‘bristles’.

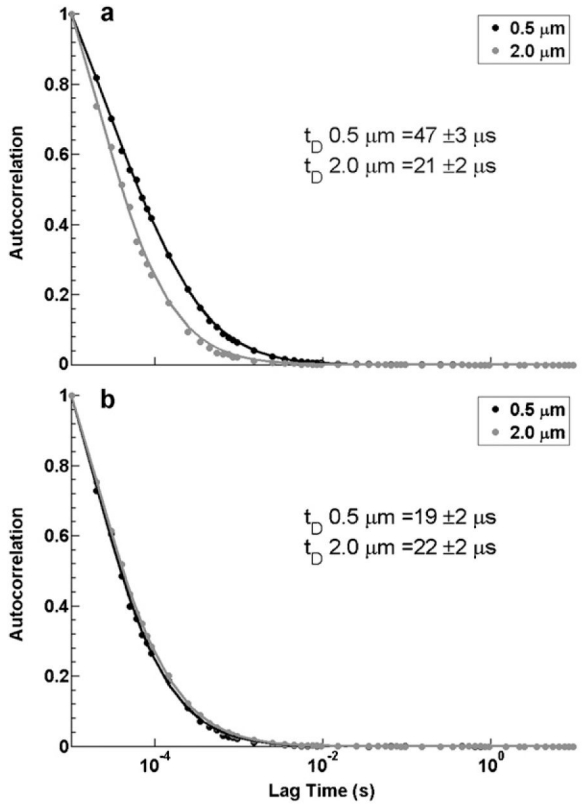

Fig. 2.

Single species averaged autocorrelation curves for R6G (a) and Alexa (b). Data sets from very close to the coverslip (0.5 μm, black) and far from the coverslip (2.0 μm, gray) are shown. The average diffusion times, with error, are also displayed. R6G displays an interaction with the surface; Alexa does not show any change in diffusion behavior near the surface.

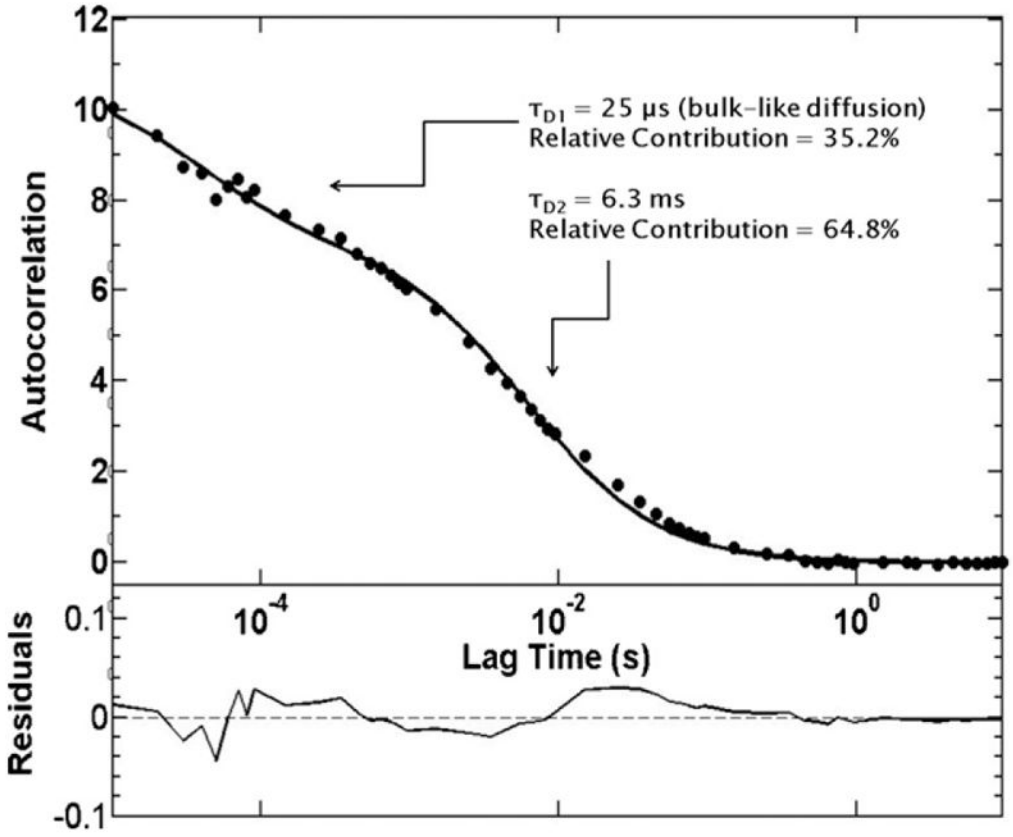

Fig. 3.

Example of an autocorrelation curve of R6G within linear PEG brush at depth of 1.0 µm fit with the two species equation. The filled circles represent the autocorrelation data and the line is the fit to the data, with residuals plotted below. The diffusion parameters show evidence of surface interaction in the significant contribution of the slow component, as compared to the bulk-like fast component (which was fit to the observed parameter of an aqueous solution).

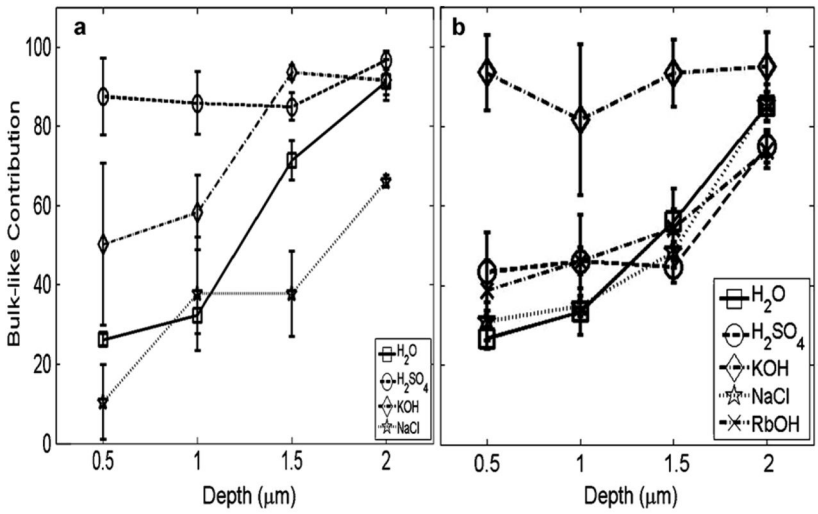

Fig. 4.

From the amplitudes of the autocorrelation curves of the data, the percent contribution of the fast, bulk-like component was determined. Here, we compare all values for all depths for R6G (a) and Alexa (b). It can be seen that an increase in the percentage of the bulk-like diffusion occurs as the focal volume shifts from the surface in nearly all cases. The lack of interaction in the acidic environment (pH 3, H_2SO_4) for cationic R6G and in the basic environment (pH 11, KOH) for anionic Alexa is shown by the high percentage of bulk-like diffusion at all depths. The aqueous (pH 6, MB water) and electrolytic (0.001 N NaCl) environments are unaffected. The same experiment was done for Alexa in an alternate base (pH 8, RbOH). The lines are included as a guide for the eye.

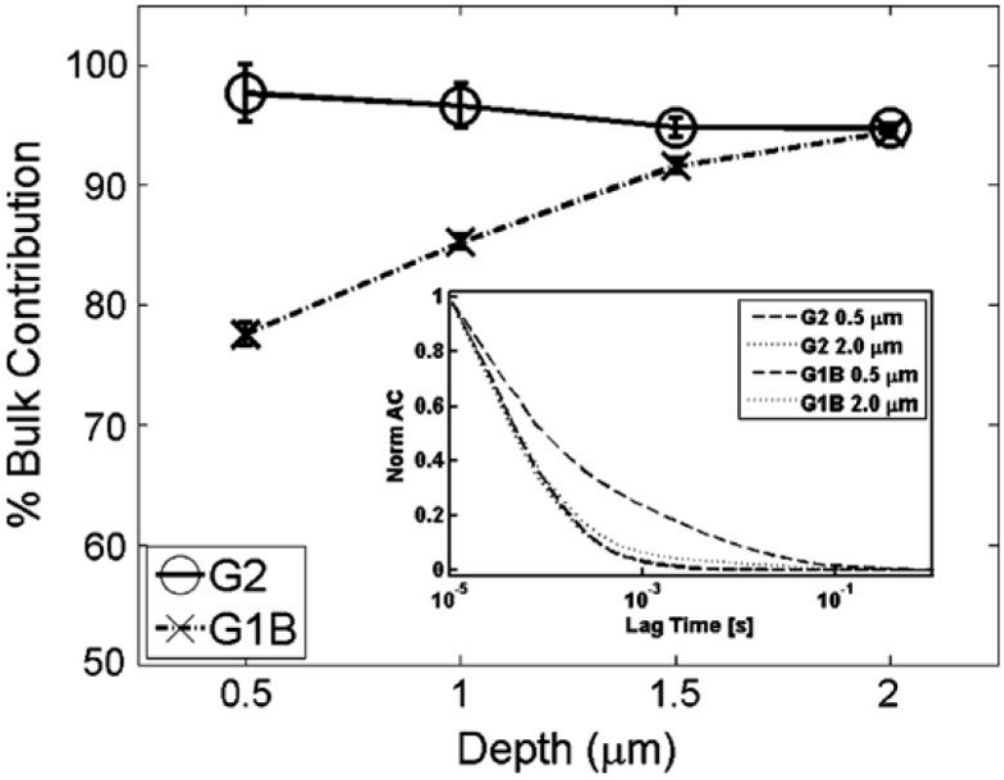

Fig. 5.

Comparison of the interaction of Alexa probe on G2 and G1B dendronized surfaces. The rising contribution of the fast, bulk-like species over the G1B dendron is indicative of the interaction of the probe with the surface. The lines are included as a guide for the eye. Inset features a comparison of the normalized autocorrelation curves for G2 and G1B dendrons at 0.5 and 2.0 μm from the surface.

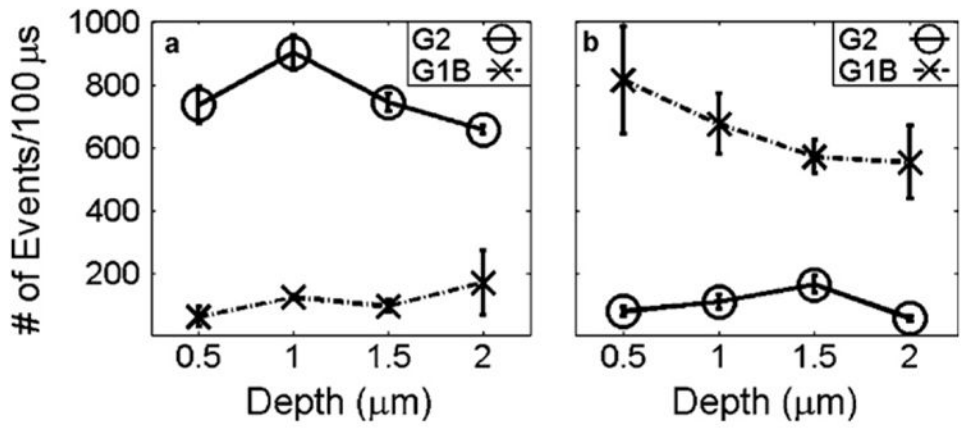

Fig. 6.

Single molecule blip frequency analysis of the Alexa-labeled α-lactalbumin (a) and free Alexa dye (b) diffusing over the G2 and G1B dendronized surfaces. The error bars for each point reflect reproducibility from multiple experiments. For the protein sample, a nearly ten-fold increase in the number of events was observed near the less-dense G2 surface as compared to the more-dense G1B surface. For the free dye sample, the opposite trend was observed. The lines are included as a guide for the eye.

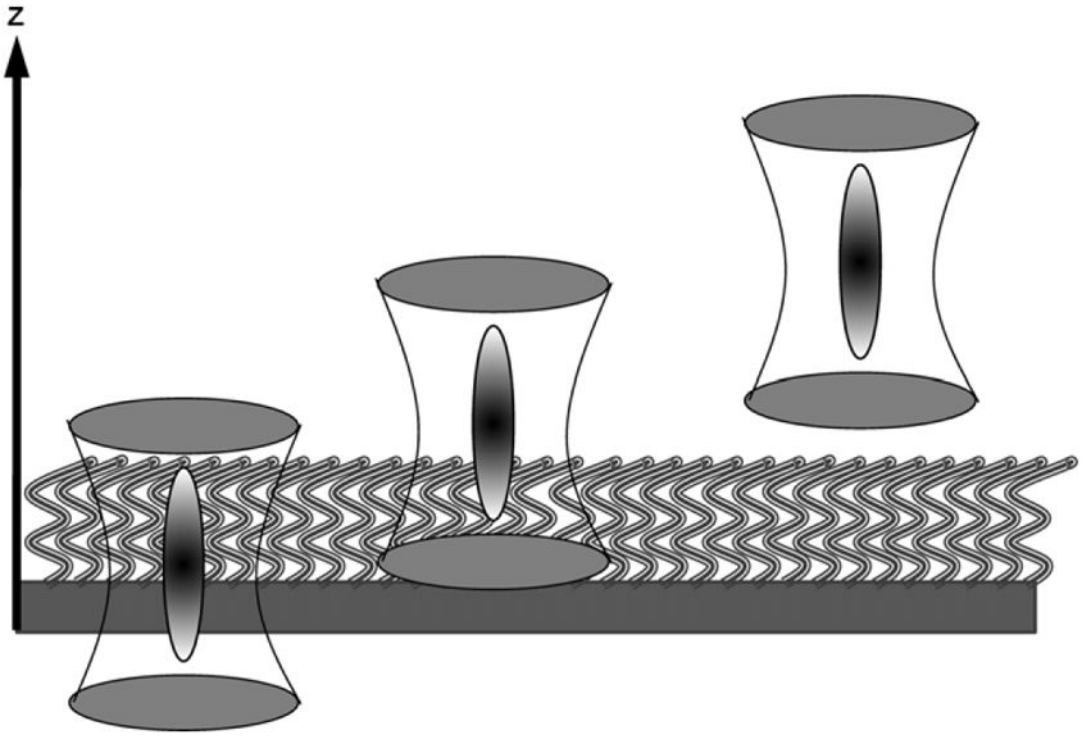

Fig. 7.

Placement of the polymerized surface with respect to the focal volume. As the focal volume is moved along the *z*-axis, the large observation volume encompasses portions of the polymer and bulk solution. Figure is not drawn to scale.

Table 1

The diffusion times of the Alexa probe in the untreated and incubated samples. The marked slowing of the probe in the incubated environment illustrates the permeability of the bottle brush polymerized surface.

Condition of sample	Slow component diffusion time
Untreated	46 ± 4 μs
Incubated	1.2 ± 0.8 ms